Materials Today Bio 17 (2022) 100461

Contents lists available at ScienceDirect

Materials Today Bio

journal homepage: www.journals.elsevier.com/materials-today-bio

A living material platform for the biomineralization of biosilica

Büşra Merve Kırpat Konak [a,1], Mehmet Emin Bakar [a,1], Recep Erdem Ahan [a], Emel Uzunoğlu Özyürek [b], Serap Dökmeci [c], Urartu Özgür Şafak Şeker [a,*]

[a] UNAM - Institute of Materials Science and Nanotechnology, Bilkent University, Ankara, 06800, Turkey
[b] Department of Endodontics, Dental Faculty, Hacettepe University, Ankara, 06100, Turkey
[c] Department of Medical Biology, Medical Faculty, Hacettepe University, Ankara, 06100, Turkey

ARTICLE INFO

Keywords:
Synthetic biology
Living materials
Biomineralization
Biosilicification
Regenerative medicine

ABSTRACT

Nature has a vast array of biomineralization mechanisms. The commonly shared mechanism by many living organisms to form hardened tissues is the nucleation of mineral structures via proteins. Living materials, thanks to synthetic biology, are providing many opportunities to program cells for many functionalities. Here we have demonstrated a living material system for biosilicification. Silaffins are utilized to synthesize silicified cell walls by one of the most abundant organism groups called diatoms. The R5 peptide motif of the silaffins is known for its ability to precipitate silica in ambient conditions. Therefore, various studies have been conducted to implement the silicification activity of R5 in different application areas, such as regenerative medicine and tissue engineering. However, laborious protein purification steps are required prior to silica nanoparticle production in recombinant approaches. In this study, we aimed to engineer an alternative bacterial platform to achieve silicification using released and bacteria-intact forms of R5-attached fluorescent proteins (FP). Hence, we displayed R5-FP hybrids on the cell surface of *E. coli* via antigen 43 (Ag43) autotransporter system and managed to demonstrate heat-controllable release from the surface. We also showed that the bacteria cells displaying R5-FP can be used in silicification reactions. Lastly, considering the stimulating effect of silica on osteogenic differentiation, we treated human dental pulp stem cells (hDPSCs) with the silica aggregates formed via R5-FP hybrids. Earlier calcium crystal deposition around the hDPSCs was observed. We envision that our platform can serve as a faster and more economical alternative for biosilicification applications, including endodontics.

1. Introduction

Biomineralization is the production of minerals by living organisms and is a frequent natural phenomenon. Common examples include the bioassembly of bone and tooth [1], spicules of demosponges [2], mollusk shells [3], diatom cell walls [4], and bacterial magnetic nanoparticles [5]. Components of these natural biomineralization systems are engineered for various purposes using synthetic biology approaches to synthesize mineralized structures for industrial and biotechnological applications. Hence, conventional inorganic methods can be replaced with biomimetic ones, which may provide faster, more efficient, environment-friendly, and biocompatible alternatives [6,7]. In this manner, many in vitro biomineralization studies are conducted. These may cover the investigation of protein nucleator dependency of particle morphology, as done with hydroxyapatite crystals [8], or the synthesis of silica biomaterials for bone regeneration applications via silicatein enzymes isolated from sponges [9]. Even tools for cancer diagnostics are being developed using magnetite accumulating ability of iron-binding proteins such as Mms6 [10].

Diatoms are a large group of microalgae that can synthesize highly ordered nanoporous cell walls from silicic acid ($Si(OH)_4$) [11]. These micropatterned cell walls, or frustules, are composed of hydrated silicon dioxide ($SiO_2{\cdot}nH_2O$) [12]. Thanks to their unique shapes and optical properties, they don't only provide mechanical protection but also enhance light-harvesting for photosynthetic reactions [13]. Frustule biomineralization happens via silica deposition on polypeptides known as silaffins, isolated from proteinaceous parts of *Cylindrotheca fusiformis* frustules. Although all three silaffin types bear many post-translational modifications (PTMs), silaffin-2 has no silica precipitation activity, unlike silaffin-1A and silaffin-1B [14]. The latter two are phosphorylated on the serine residues and attached to long-chain polyamines (LCPAs) by the lysine residues [14,15]. These PTMs are negatively charged. Thus function

* Corresponding author.
E-mail address: urartu@bilkent.edu.tr (U.Ö. Şafak Şeker).
[1] These authors have contributed equally.

https://doi.org/10.1016/j.mtbio.2022.100461
Received 13 July 2022; Received in revised form 30 September 2022; Accepted 8 October 2022
Available online 10 October 2022

as the nucleation sites for metal ions, which are positively charged [14]. Sequencing studies showed that silaffin-1A includes repetitions of a specific polypeptide motif, SSKKSGSYSGSKGSKRR(I/N)L, called R5 [14]. It has been demonstrated that synthetic R5 alone, lacking PTMs, can quickly cause silica to precipitate from silicic acid solutions [16]. This rapid silicifying activity of R5 in physiologically relevant conditions makes it a good candidate for many biotechnology applications.

Silica-based materials are used widely in endodontic and orthopedic applications as dental cement and bone substitutes. These include tricalcium silicate-based cements [17], and nano-fibrous gelatin/silica bioactive glasses [18]. Besides the structural usage as a filling material, proliferation and differentiation stimulating effects of silica on osteoblasts and dental pulp stem cells (DPSCs) are also known [17–19]. Hence, the silicifying activity of R5 can be functionalized in regenerative medicine applications [20]. Additional examples of the potential uses of R5 include enzyme/protein immobilization studies [21,22] and fluorescent biodot synthesis [23]. In these studies, purification of R5-conjugated oligopeptides and hybrid proteins generally relies on affinity chromatography techniques via recombinantly attached genetic tags [21,22,24]. Although purification methods, such as silica resins [23], are available and eliminate the need for fused tags, faster and more economical alternatives are required. Recently, filamentous bacteriophages displaying R5 on their surface are shown to be able to precipitate silica [25]. Similarly, we aimed to utilize a bacterial surface display system to display R5 and conduct silica precipitation reactions.

Antigen 43 (Ag43) is an abundant surface protein of *Escherichia coli*. (*E. coli*) The translated Ag43 comprises an N-terminus signal peptide, an autochaperone domain, an α-passenger domain, and a β-translocation domain. Since Ag43 is an autotransporter, it is self-sufficient for its transport and secretion [26,27]. While the signal peptide enables transport to the periplasmic space, the β-subunit forms a β-barrel structure and is inserted into the outer membrane, forming a pore-like integral structure (Fig. 1) [28]. The folding of the α-passenger domain is facilitated by the autochaperone domain. Upon its folding, the α-passenger domain is transported to the surface via the β-subunit. The autochaperone domain remains covalently attached to the β-barrel, whereas the α-passenger domain is noncovalently attached (Fig. 1) [26,27]. The self-recognition ability of the secreted α-domain causes auto-aggregation of the bacteria colonies when secreted. This self-recognition ability is accomplished by the first 160 amino acid residues at the N-terminus [29]. It has been shown that these residues can be replaced by the protein of interest (POI), and the POI can be displayed on the bacteria cell surface [30].

In this study, we aimed to develop a novel route to display and secrete R5 peptide and provide a fast alternative for its purification (Fig. 1). Therefore, an engineered Ag43 autotransporter is utilized to deliver R5-FP hybrids to the *E. coli* cell surface. Silicification activities of both the secreted and surface-intact forms of R5 fusions are demonstrated. Silicified R5-FP is found to be causing earlier deposition of extracellular calcium nodules around the human dental pulp stem cells, which might indicate an increase in their osteogenic potential. Therefore, we envision that our biosilicification platform can be used as an alternative silica-nucleating platform in regenerative medicine applications.

2. Results and discussion

2.1. Construction, display, and release of R5-sfGFP hybrid via Ag43

Conventional affinity chromatography techniques used for R5

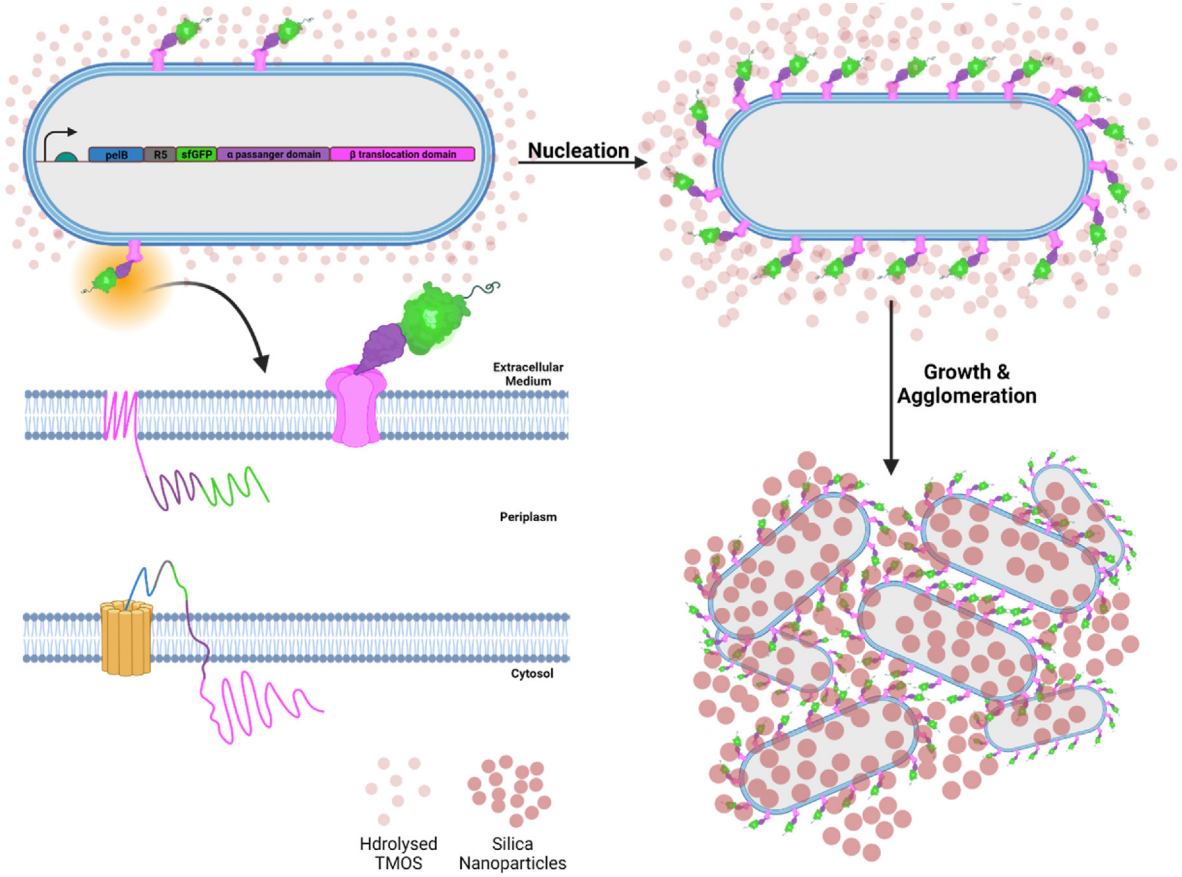

Fig. 1. Graphical illustration depicting the antigen 43-mediated secretion of R5-FP constructs and the subsequent formation of silica nanoparticles from hydrolyzed silica precursor (TMOS) via bacteria-intact R5-FP. pelB signal peptide (blue), β-translocation domain (pink), α-passenger domain (purple), sfGFP (green), and R5 peptide (black) are shown. Created with BioRender.com.

purification are laborious, and affinity tags remain intact in the purified protein constructs. To circumvent extensive purification steps, and provide a faster alternative, R5-FP (Fluorescent Protein) hybrids are aimed to be displayed on the cell surface via the Ag43 (Antigen 43) autotransporter system. We used an engineered version of Ag43 in which the first 160 amino acids of the α-subunit are deleted, hence named 160 N. Deleted subunits can be replaced with cargo proteins [30]. Therefore, we first genetically constructed an Ag43-sfGFP-R5 hybrid and inserted it into an isopropyl β-D-1-thiogalactopyranoside (IPTG)-inducible vector (Fig. S5), and transformed it into *E. coli* BL21 (DE3) cells. Upon reaching the cell surface, the α-subunit of Ag43 faces the cell exterior and becomes noncovalently attached to the membrane-embedded β-subunit (Fig. 1). Along with its cargo, the α-subunit can be detached by heating it to 60 °C [31]. We induced the cells with IPTG and applied heat incubation at 60 °C, expecting the release of hybrid protein formed by 160N-R5-sfGFP (~68 kDa) to the external media. We successfully showed the presence of the released hybrid proteins in the media via Western blot analysis (Fig. 2A). However, a strong signal from a band corresponding to ~35 kDa also appeared. Most probably, this is the R5-sfGFP detached from the Ag43 α-subunit during the sample preparation steps. For further confirmation, the fluorescence signal levels of the supernatants were compared (Fig. 2B). Although there is a significant increase in the signals of the induced cells, an expression leakage from the promoter is observed with the uninduced cells. A minimal heat-independent detachment of the cargo is also observed for induced and uninduced cells. Lastly, we conducted immunocytochemistry (ICC) analysis to show the successful display of R5-sfGFP on the cell surface (Fig. 2C). In this manner, an anti-his antibody conjugated with Dylight550 is utilized. Green emission from the R5-sfGFP and red emission from the Dylight 550 successfully confirmed the presence of surface-intact R5-sfGFP. Thus, we successfully showed the surface display of R5-sfGFP via Ag43 and demonstrated its heat-controllable release.

2.2. Silicification via released R5-sfGFP hybrid proteins

Next, we checked the silicification-inducing ability of the R5-FP hybrids via transmission electron microscopy (TEM) and energy-filtered TEM (EFTEM). Although native silaffin-1A conserves its precipitating activity at pH values down to 4.0, the R5 peptide loses its activity under pH 6.0 [32]. In vitro precipitation experiments showed that pH values greater than or equal to 7.0 are optimal for silica precipitation when R5 is used alone or fused to GFP [21,33]. Thus, the silicification reaction is conducted in silica precipitation buffer with pH 8.0, including hydrolyzed TMOS (tetramethyl orthosilicate) as the silica precursor [34]. Previous works have shown that unmodified R5 peptides can nucleate SiO_2 nanoparticle formation in vitro. Generally, these particles have spherical morphologies with an average diameter of 500–600 nm [35,36]. Fluorescent markers and enzymes are fused with silaffins for various purposes, such as enzyme immobilization and biodot synthesis [23,37,38]. The silicification activity of R5 is not affected when it is fused to GFP, mCherry, or YFP, and spherical nanoparticle morphology was also conserved in these studies [23,38]. However, we suspected that the conventional spherical morphology of the silica precipitates might be disrupted with our R5-FP hybrids since the α-subunit of Ag43 remains attached to the hybrids upon the release. With this in mind, first, the surface-displayed R5-sfGFP is released via heat incubation from the induced cells, and the supernatants were used in the silica precipitation reaction (Fig. 3A). As we suspected, although some parts of the silica precipitates include spherical-like particles in the nanometer range, the general structure appeared as an aggregated amalgamation of these spherical particles. Even though similar aggregated morphology was observed in the positive controls, which are precipitated via 10% PEI (polyethylenimine, flocculating agent of silica [39]), spherical particle formation was more prominent and prevalent in these as expected (Fig. 3B). The elemental origin of the nucleated aggregates was shown by energy-dispersive X-ray spectroscopy (EDS) and energy-filtered TEM (EFTEM). While the Si peaks in the EDS graphs reflect the presence of silicon atoms, C and O peaks indicate the presence of the organic molecules in the same area (Fig. 3A). This was further supported by the EFTEM results, where the C, O, and P signals overlap with the Si signals (Fig. 3E). Expectedly, the EDS count of silica was greater with the positive control (Fig. 3B). Since we observed a minimal release from the

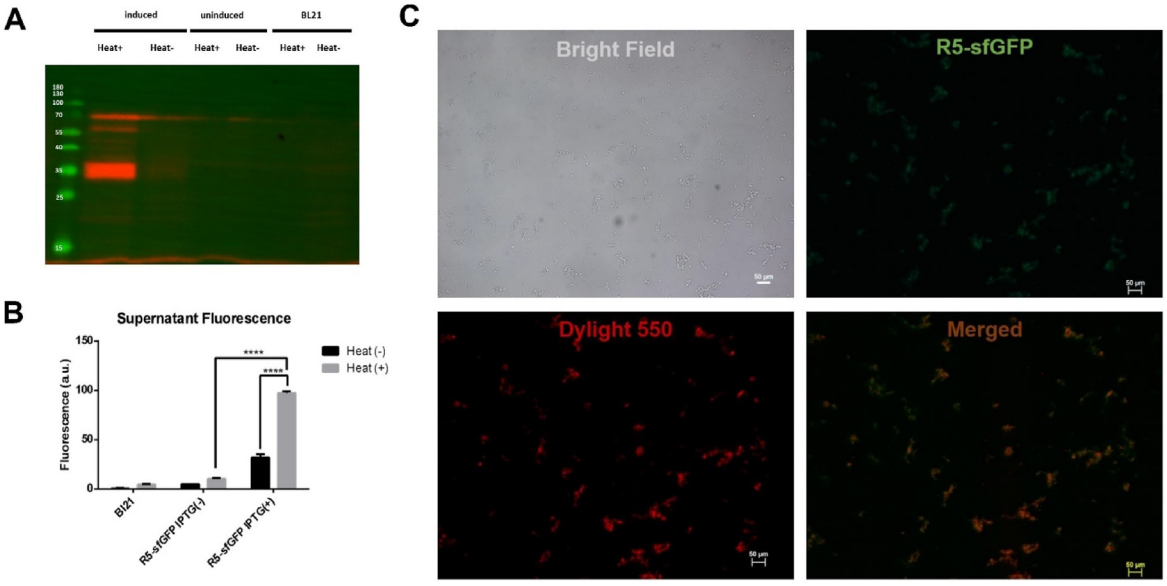

Fig. 2. (A) Western blot analysis conducted from the supernatants of induced and uninduced R5-sfGFP expressing cells. Cells incubated with and without heat are indicated. BL21 cells were used as the negative control. The first lane shows the ladder. Corresponding protein weights are marked and are in kDa (expected molecular weight: 68 kDa). (B) Fluorescence changes in cell supernatants by heat incubation for analysis of the expression of R5-sfGFP protein on the cell surface. The obtained results were analyzed by two-way analysis of variance (ANOVA) (GraphPad Prism v6); the differences between the groups were marked with "*" ($p \leq 0.05$, $p \leq 0.01$, $p \leq 0.001$, and $p \leq 0.0001$ respectively represented by "*", "**", "***" and "****"). No markings were included for the groups that did not show significant differences. (C) ICC (immunocytochemistry) experiment was done for the displayed R5-sfGFP protein with an anti-his antibody conjugated with Dylight550. Fluorescent microscopy images are shown (bars: 50 μm).

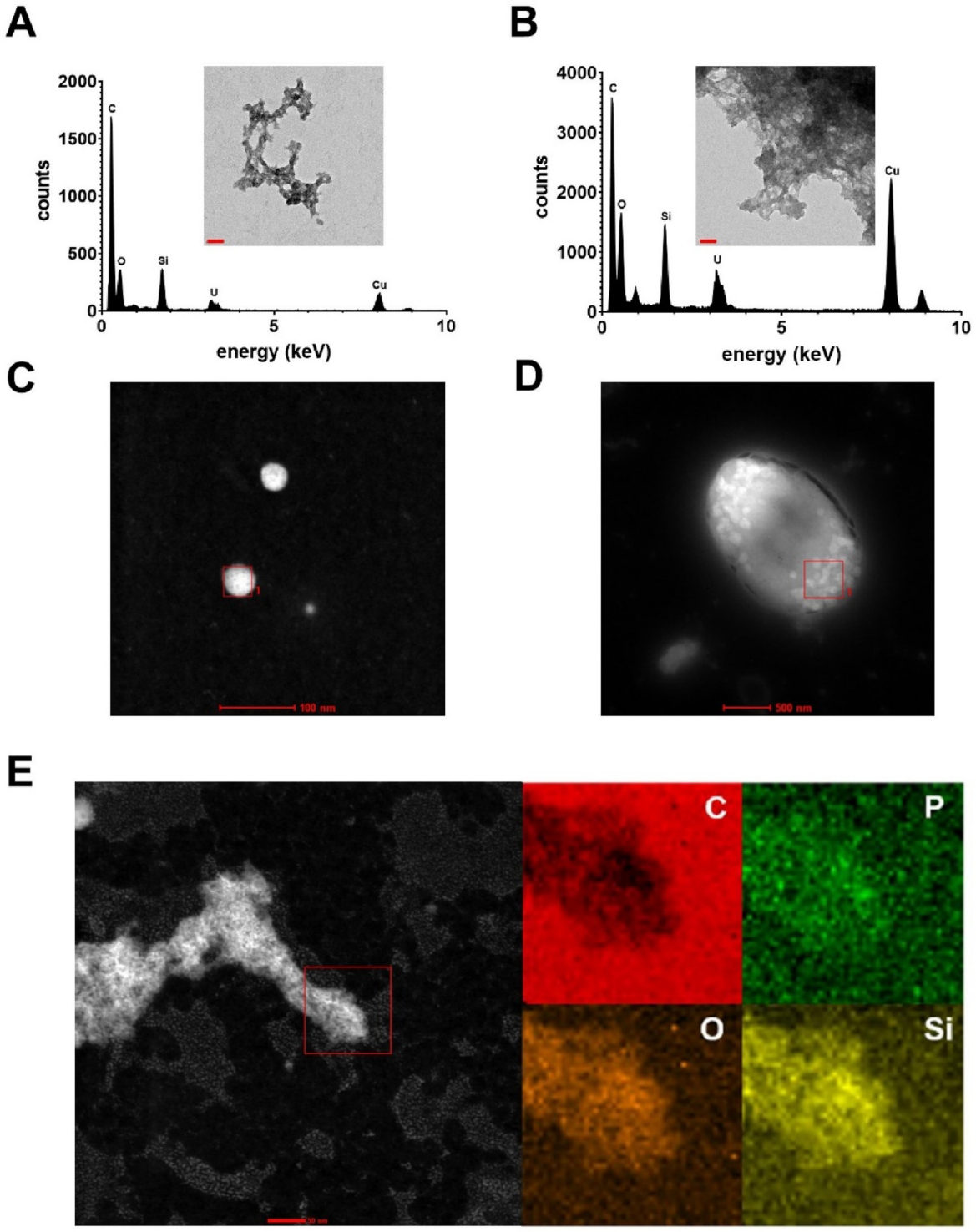

Fig. 3. Transmission electron micrographs (TEM) taken after the silica precipitation reactions using (A) the supernatant of induced cells expressing R5-sfGFP, (B) 10% PEI, (C) supernatant of uninduced cells expressing R5-sfGFP, (D) pellet of induced cells expressing R5-sfGFP. Red bars in (A), (B), (C), and (D) correspond to 50, 50, 100, and 500 nm respectively. Energy-dispersive X-ray spectroscopy (EDS) results for (A), and (B) are given. EDS results of (C) and (D) are collected from the areas indicated with the red squares, and the results are provided in the supplementary data (Fig. S7). (E) Energy-filtered TEM (EFTEM) results for the silica precipitated with the supernatant of induced cells expressing R5-sfGFP. The area indicated with the red square is used for the elemental analysis of C, O, P, and Si. Corresponding elemental filters are indicated in the figure. Graphical images show the areas where the X-ray signal was collected. The red bar corresponds to 50 nm.

uninduced cells (Fig. 2B), supernatants of heat-incubated uninduced cells were also used in the precipitation reaction (Fig. 3C). Although spherical particles are formed and contain silica, as confirmed by EDS (Fig. S7), they were significantly infrequent, and may originate from the leaky expression or spontaneous formation of silica nanoparticles. Conservation of the spherical morphology in these samples compared to the aggregates formed by R5-sfGFP, might reflect that the higher concentration of α-subunit-R5-sfGFP hybrid interferes with the spherical morphology.

We also used induced cells directly without heat incubation in the precipitation reaction to check the presence of the silica nanoparticles on the cell surface by TEM. There were many well-distinguished spherical particles on the bacteria membranes, and EDS confirmed that they contain silica (Fig. S7).

2.3. Silicification via surface-displayed R5-FP hybrid proteins

Next, we examine the silica nanoparticle formation ability of the surface-attached R5-FP hybrids without detachment from the surface. To check the silica precipitation activity of fluorescent markers other than sfGFP, the R5 peptide is also fused to YFP (yellow fluorescent protein) and mCherry. Western blot and SDS-PAGE analyses of R5-YFP and R5-mCherry hybrids confirmed their release upon heat incubation (Fig. S6). The silica precipitation reaction was conducted with induced cells and precipitates imaged via scanning electron microscopy (SEM). Because the silicification reaction is conducted in the presence of bacteria cells, we were not expecting to observe ordered structures. SEM images confirmed our expectations (Fig. 4C). As the controls, silica precipitation reactions were also conducted with the uninduced cells for each fluorescent marker. Unlike the induced cells, uninduced and negative controls lack aggregated silica structures (Fig. S8). Therefore, the bacteria cells were well-distinguished in the controls. The presence of silica along with the organic molecules is shown for R5-sfGFP via SEM and elemental maps obtained via EDS (Fig. 4A). Further SEM and EDS analyses were also conducted for all three silicified cell lines, yielding sharp silica peaks for each (Fig. 4C), which are lacked by the uninduced and negative controls (Fig. S8). Silicified structures were analyzed from different points of view and magnification rates to demonstrate biosilicification, which was facilitated by all three bacteria strains. While a panoramic view of the bacteria-induced silica aggregates is shown in Fig. 4C–(a) for R5-sfGFP, formation of the bacteria-embedded silica aggregates can be well observed in the R5-mCherry images (Fig. 4C–(e-f)). We also wanted to check the presence and conservation of the fluorescent signals. Hence, we utilized confocal microscopy and successfully showed that silica precipitated via all the surface-intact R5-FP hybrids emitted fluorescence signals (Fig. 4B). With this, we demonstrated that the fluorescently active surface-intact R5-FP hybrids can precipitate silica from silica precursors in vitro.

2.4. Osteogenic stimulation of hDPSCs via R5-sfGFP-nucleated silica structures

Upon verifying the silicification activity of our constructs, we wanted to test the potential of R5-FP nucleated silica in regenerative medicine applications, specifically in endodontics. Since dental implants, including silica, enhance the differentiation of human dental pulp stem cells (hDPSCs), we decided to utilize hDPSC in the subsequent experiments [18]. In this manner, hDPSCs were grown in proliferation medium. Then the media is replaced with osteogenic medium containing R5-sfGFP nucleated silica. Previous studies showed that the osteogenic medium stimulates osteogenic differentiation via increasing the expression of osteoblastic markers, such as ALP (alkaline phosphatase) [40]. Although there is no consensus on the differentiation period of hDPSCs [17,40,41], extracellular mineral matrix nodules are observed by day 30 around the DPSCs cultured in osteogenic medium [40]. Considering the differentiation-inducing effect of silica, we expected to observe calcium depositions around the silica-treated cells earlier than the controls. We conducted alizarin red staining on days 7, 14, 21, and 28 to check calcium crystal formations. Even though local red aggregates are observed rarely in the silica-treated cells upon alizarin red staining, their rarity in the culture plate did not change from day 7–28 (Fig. 5). Hence, we suspect that these might not be the calcium crystals. During the staining procedure, silica particles in the culture probably accumulated alizarin red physically rather than chemically, as in the case of calcium. However, the staining results of day 28 revealed a very dense and extensive network of calcium nodules. The mineralized calcium deposits had a scattered distribution around the cell culture, indicated by the local accumulations of calcium (Fig. 5). This heterogeneous deposition might be originated from the unequal exposure of the cells to the R5-sfGFP-nucleated silica aggregates. No extracellular deposits were visible around the controls. These results reflect the differentiation-inducing effect of the silica nucleated by R5-sfGFP.

3. Conclusions

To our knowledge, bacterial surface display of R5 for in vitro silica nucleation is accomplished for the first time in this study. We have utilized an engineered antigen 43 autotransporter system to secrete R5-FP hybrids into the environment and showed that release from the surface is possible via heat-dependent detachment. The secreted R5-sfGFP hybrids were shown to be able to precipitate dissolved silica. We have also shown that bacteria with surface-intact R5-sfGFP, R5-YFP, or R5-mCherry are able to nucleate silica aggregates. Therefore, bacteria-embedded silicified structures were obtained. Hence, bacteria function both as a structural and silicifying component. Although our biomineralization platform can be used for many biotechnological applications, we first wanted to test its potential in endodontics since silica is known to induce osteoblastic transformation. In this manner, we have treated human dental pulp stem cells (hDPSC) with the silica nucleated via R5-sfGFP hybrid. Extracellular calcium crystal nodules around the cells were visible by day 28. Thus, osteogenic differentiation is possible in the presence of R5-sfGFP-nucleated silica. Our biosilicification platform provides a faster, more economical, and environment-friendly alternative purification route for silica nanoparticle synthesis.

4. Materials and methods

4.1. Plasmid construction

To construct pET22b(+) PelB 6xHis R5-sfGFP Ag43, BMK5 and REA34 primers were used in PCR reaction to insert GS linker and part of R5 sequences to upstream of sfGFP by using pET22b(+) PelB 6H Ag43 160 N sfGFP plasmid as a template [30]. To complete the insertion of R5 sequence and also addition of a BamHI restriction enzyme site, BMK6 and REA34 primers were used in the reaction by using the PCR product as the template. The PCR product and the template plasmid were digested with BamHI and AflII restriction enzymes (NEB) and then the digested fragments were ligated by T4 ligase (NEB). To construct pET22b(+) PelB 6xHis mCherry R5 Ag43 and pET22b(+) PelB 6xHis YFP R5 Ag43, pZa mCherry 3x GS linker R5 and pZa YFP 3x GS linker R5 vectors [23] were used as a template, respectively. BMK39-BMK41 primers were used to amplify mCherry 3x GS linker R5 and the backbone was amplified with BMK42 and BMK43. For the amplification of YFP 3x GS linker R5, BMK39-BMK40 primers were used. Then, BMK43-BMK44 primers were used to amplify the backbone. pET22b (+) PelB 6xHis R5-sfGFP Ag43 plasmid was used as a template for the backbone in PCR reactions. The PCR products were assembled via the Gibson Assembly method. *E. coli* DH5α PRO strain was used to transform the plasmids. After verification of the cloned plasmids, the plasmids were transformed into *E. coli* BL21(DE3) strain to express proteins. The Sanger sequencing results are given in Fig. S1, and the plasmid maps for the constructs are given in Figs. S2–4. All the DNA sequences and primer sequences used are given in Table S1 and Table S2, respectively.

4.2. Expression and characterization of the recombinant proteins

Bacteria cultures were grown in LB medium supplied with 100 μg/ml ampicillin at 37 °C, 200 rpm for overnight. The overnight cultures were diluted into fresh LB medium with a 1:100 ratio. They were grown at 37 °C, 200 rpm until their OD600 values reached ~0.4.1 mM of IPTG was added to the cultures to induce protein expression at 18 °C, 200 rpm for overnight.

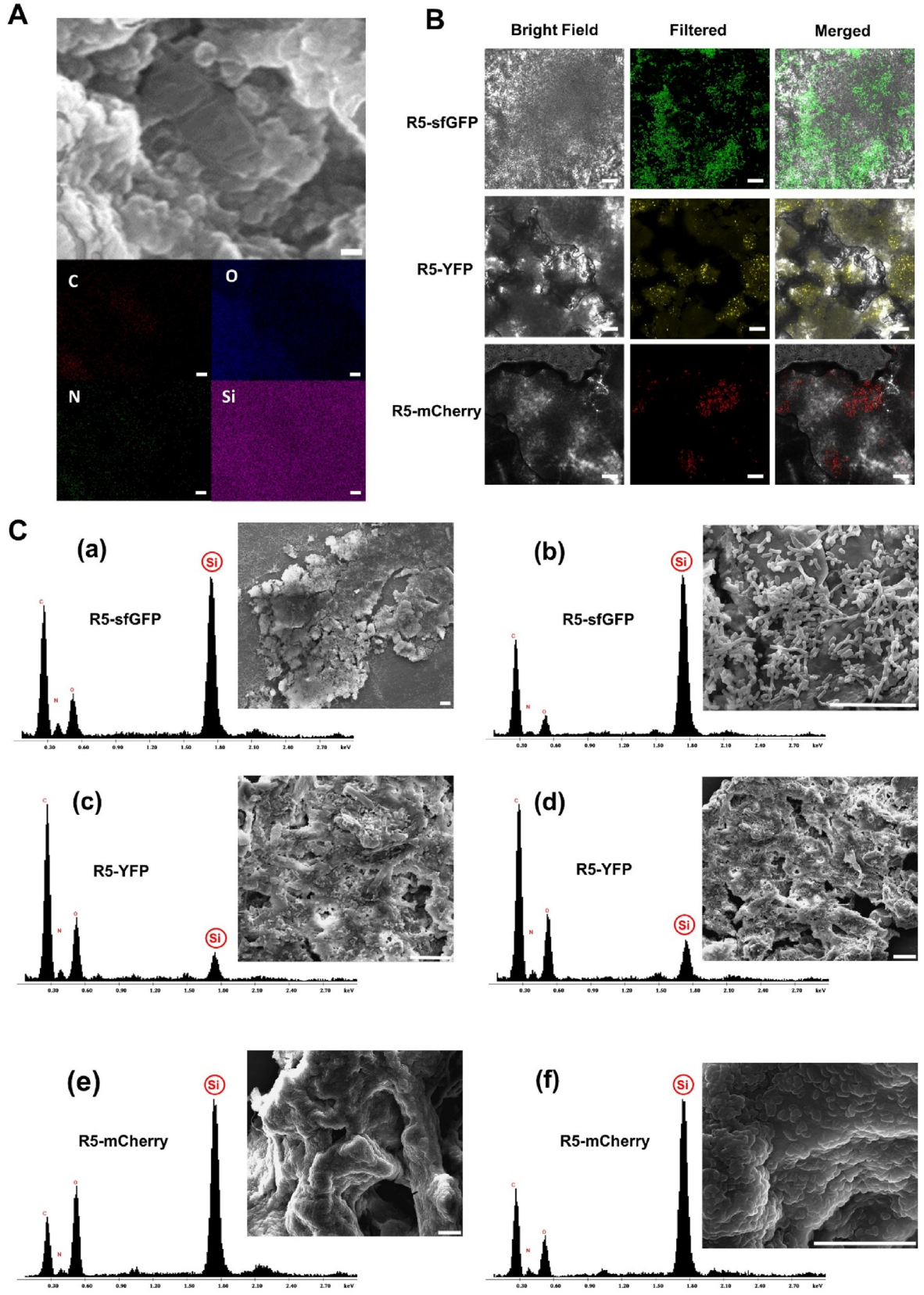

Fig. 4. Analysis of the silica precipitation ability of the cells displaying surface-intact R5-FP hybrids. (A) Scanning electron micrograph (SEM) and energy-dispersive X-ray spectroscopy (EDS) results of the same area after silica precipitation reaction using induced cells expressing R5-sfGFP. Corresponding elemental filters are indicated in the figure. White bars correspond to 200 nm. (B) Confocal microscopy images were taken after the silica precipitation reactions using cells expressing R5-sfGFP, R5-YFP, and R5-mCherry. Bright field, filtered, and merged images are indicated. White bars correspond to 20 μm. (C) SEM and EDS analysis results were taken after the silica precipitation reactions using induced cells expressing R5-sfGFP (a–b), R5-YFP (c–d), and R5-mCherry (e–f). C, O, N, and Si peaks are marked. Silica peaks are indicated with the red circles. White bars correspond to 10 μm.

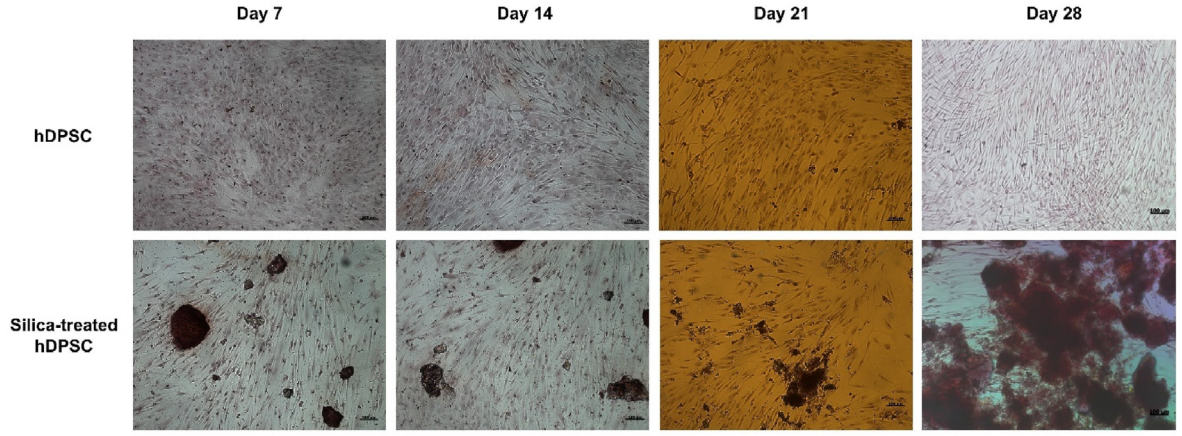

Fig. 5. Light microscopy images of human dental pulp stem cells (hDPSCs) and silica-treated hDPSCs after alizarin red staining. Images were taken at days 7, 14, 21, and 28. Black bars correspond to 100 μm.

After induction, 10^9 cells were centrifuged and the pellets of culture were washed with 1x PBS and then resuspended in 250 μl of 1x PBS. Resuspended cells were incubated at 60 °C for 5 min and they were centrifuged at 14000 rpm for 5 min. Fluorescence signals of 200 μl of the supernatants as triplicates were measured by an M5 spectrophotometer and also the supernatants were used for Western blot/SDS-PAGE analysis. Samples were boiled at 95 °C for 5 min and they were run in 4% stacking and 12% separating gel at 120 V. Either the gel was stained with Coomassie Blue or transferred to PDVF membrane with Bio-RAD turboblot device. The membrane was incubated in %5 milk powder dissolved in TBS-T buffer for blocking. The membrane was incubated with goat anti-His primary antibody with a 1:5000 dilution ratio at 4 °C overnight. After the washing steps, the membrane was incubated with an anti-goat secondary antibody conjugated with HRP with a 1:5000 ratio. Images were taken in Bio-RAD ChemiDoc by using Bio-RAD ECL substrate kit.

For the immunocytochemistry (ICC) experiment, 250 μl of cultures were centrifuged and washed with 1X PBS. The pellets were resuspended in 250 μl of 1% BSA in PBS-T solution for blocking at room temperature for 2 h on a rotator. After incubation, the blocking solution was replaced by a primary mouse anti-his antibody diluted at a 1:250 ratio in 1% BSA-PBS-T solution and they were incubated at 4 °C for overnight on the rotator. The primary antibody solution was removed by washing with 1x PBS for 3 times. As the secondary antibody solution, anti-mouse antibody conjugated DyLight550 diluted with a 1:500 ratio in 1% BSA-PBS-T was used and cells were incubated with the solution at room temperature for 2 h. After cells were washed with PBS twice, they were analyzed under the epifluorescence microscope.

4.3. In vitro silica synthesis using the recombinant proteins

For silica synthesis, the strain having pET22b(+) 6xHis R5-sfGFP Ag43 vector was induced as described above. Either the supernatant of heat-treated cells or the cells were used to synthesize silica. 10^{10} number of cells were centrifuged and washed with ddH2O for two times. The pellets were resuspended in 200 μl of ddH2O. 1.6 ml of silica precipitation buffer solution (0.1 M NaOH, 0.1 M KH_2PO_4, pH 8) and 200 μl of 1 M TMOS dissolved in 1 mM HCl were mixed with the cells. The reaction was incubated at room temperature for 30 min on the rotator. The supernatant was discarded by centrifugation and the pellet was washed twice with the wash buffer solution (0.25 M NaOH, 0.25 M KH_2PO_4, pH 7). The pellet was sonicated for 30 min at room temperature and was resuspended in 100 μl of ddH2O. The samples were analyzed via ESEM (FEI Quanta), TEM (Fei Technai), and confocal microscope (Leica) imaging. Instead of cells, 10% PEI was used in the reaction as the positive control, and the strain without the plasmid and uninduced cells were used as the negative control. For silica synthesis with released R5-sfGFP proteins, cells were first treated with heat as described above and their supernatants were taken to use in the precipitation reactions. Silica was synthesized at a larger volume when it was used for cell culture experiments.

4.4. Cell culture experiments

DPSCs were grown in growth medium (DMEM low glucose, 10% FBS, 1% Penicillin, Streptomycin, and L-Glutamine) at 37 °C with %5 CO2 in the incubator. After the cells reached 90% confluency, the medium was discarded and the cells were washed with 1X PBS twice. Cells were detached by trypsin treatment. The number of cells was measured via hemocytometer and one hundred thousand cells were added in 3 ml of medium in each well of the 6-well plate. When their confluence reached 60%, 1 mg/ml of silica is dried by a critical Point Dryer (CPD) and then dissolved in water containing % 0.05 BSA and osteogenic medium (DMEM low glucose, 10% FBS, 1% PenStrep, 10 mM β glycerophosphate, 100 nM dexamethasone, 0.2 mM ascorbic acid) was replaced with the growth medium. The calcium deposits were checked by Alizarin Red Staining at 7., 14., 21. and 27. day. The culture medium of the cells was removed and the wells were washed with 1x PBS three times. Cells were fixed with 1 ml of 4% formaldehyde for 15 min at room temperature. The cells were washed three times with 2 ml of ddH2O after removing the fixative. 1 ml of 40 mM Alizarin Red S was added to each well and then cells were incubated at room temperature for 30 min with gentle shaking. After incubation, the dye was removed and the cells were washed five times with ddH_2O. Wells were analyzed under the inverted light microscope.

For SEM imaging, 1 μl of samples were dropped cast on glass substrates which were 40 μm of gold deposited by thermal evaporation and air-dried for 30 min at room temperature. The surface of the samples was covered with gold-palladium which has a thickness of around 5 nm. Images were taken at different forward voltages for electron energy (5-20 keV). For TEM imaging, 15 μl of samples were dropped on a parafilm surface and the carbon-coated surface of an EMS Ni grid with formvar/C support (300 mesh) was put on top of the samples drops for 1-min incubation. The excess amount of samples was taken by touching the side of the grids to tissue paper. The grids were washed with drops of water three times. 2% uranyl acetate was used to stain the samples for 30 s. Electron acceleration power was 200 keV. To identify the material composition, Energy-dispersive X-ray spectroscopy (EDAX Genesis software) was also performed.

4.5. Statistical analysis

All the data given in the graphs were drawn by using the "GraphPad Prism v6" software with the principle of "mean ± standard error mean"

and two-way analysis of variance (ANOVA) was used for data analysis. Trial track changes.

Credit author statement

UOSS formed the idea and designed the experimental work, BMKK designed experimental work, analyzed data, REA, MEB helped with the cloning and display experiments, MEB and BMKK carried out electron microscopy work, EUO and SD isolated cells and characterized them. BMKK carried out cell culture experiments. UOSS, BMKK, prepared the initial draft. All of the authors prepared the final version of the manuscript.

Declaration of competing interest

The authors declare the following financial interests/personal relationships which may be considered as potential competing interests:Urartu Ozgur Safak Seker reports financial support was provided by Scientific and Technological Research Council of Turkey. None.

Data availability

Data will be made available on request.

Acknowledgement

This study was suppoorted by The Scientific and Technological Research Council of Turkey (TUBITAK) Grant Number : 115M108.

Appendix A. Supplementary data

Supplementary data to this article can be found online at https://doi.org/10.1016/j.mtbio.2022.100461.

References

[1] C.S. Kovacs, C. Chaussain, P. Osdoby, M.L. Brandi, B. Clarke, R.v. Thakker, The role of biomineralization in disorders of skeletal development and tooth formation, Nat. Rev. Endocrinol. 17 (2021) 336–349, https://doi.org/10.1038/s41574-021-00488-z, 6. 17 (2021).

[2] W.E.G. Müller, A. Boreiko, X. Wang, S.I. Belikov, M. Wiens, V.A. Grebenjuk, U. Schloßmacher, H.C. Schröder, Silicateins, the major biosilica forming enzymes present in demosponges: protein analysis and phylogenetic relationship, Gene 395 (2007) 62–71, https://doi.org/10.1016/J.GENE.2007.02.014.

[3] A.G. Checa, Physical and biological determinants of the fabrication of Molluscan shell microstructures, Front. Mar. Sci. 5 (2018) 353, https://doi.org/10.3389/FMARS.2018.00353/BIBTEX.

[4] E.V. Armbrust, The life of diatoms in the world's oceans, Nature 459 (2009) 185–192, https://doi.org/10.1038/nature08057, 7244. 459 (2009.

[5] C.-D. Yang, H. Takeyama, T. Tanaka, A. Hasegawa, T. Matsunaga, Synthesis of Bacterial Magnetic Particles during Cell Cycle of AMB-1, Twenty-Second Symposium on Biotechnology for Fuels and Chemicals, 2001, pp. 155–160, https://doi.org/10.1007/978-1-4612-0217-2_13.

[6] M. Dade-Robertson, C.R. Figueroa, M. Zhang, Material ecologies for synthetic biology: biomineralization and the state space of design, Comput. Aided Des. 60 (2015) 28–39, https://doi.org/10.1016/J.CAD.2014.02.012.

[7] I. Hussain, N.B. Singh, A. Singh, H. Singh, S.C. Singh, Green synthesis of nanoparticles and its potential application, Biotechnol. Lett. 38 (2016) 545–560, https://doi.org/10.1007/S10529-015-2026-7/FIGURES/3.

[8] E. Duman, E. Şahin Kehribar, R.E. Ahan, E. Yuca, U.Ö.Ş. Şeker, Biomineralization of calcium phosphate crystals controlled by protein-protein interactions, ACS Biomater. Sci. Eng. 5 (2019) 4750–4763, https://doi.org/10.1021/ACSBIOMATERIALS.9B00649/ASSET/IMAGES/LARGE/AB-2019-00649A_0007. JPEG.

[9] S. Wang, X. Wang, F.G. Draenert, O. Albert, H.C. Schröder, V. Mailänder, G. Mitov, W.E.G. Müller, Bioactive and biodegradable silica biomaterial for bone regeneration, Bone 67 (2014) 292–304, https://doi.org/10.1016/J.BONE.2014.07.025.

[10] M. Yavuz, M. Ütkür, Ş. Kehribar, E. Yağız, Ü. Sarıtaş, U. Özgür, Ş. Şeker, M. Yavuz, E.Ş. Kehribar, U.Ö.Ş. Şeker, M. Ütkür, E. Yağız, E.Ü. Sarıtaş, Engineered bacteria with genetic circuits accumulating nanomagnets as MRI contrast agents, Small 18 (2022), 2200537, https://doi.org/10.1002/SMLL.202200537.

[11] C.W.P. Foo, J. Huang, D.L. Kaplan, Lessons from seashells: silica mineralization via protein templating, Trends Biotechnol. 22 (2004) 577–585, https://doi.org/10.1016/J.TIBTECH.2004.09.011.

[12] R.W. Drum, R. Gordon, Star Trek replicators and diatom nanotechnology, Trends Biotechnol. 21 (2003) 325–328, https://doi.org/10.1016/S0167-7799(03)00169-0.

[13] M.A. Ferrara, P. Dardano, L. de Stefano, I. Rea, G. Coppola, I. Rendina, R. Congestri, A. Antonucci, M. de Stefano, E. de Tommasi, Optical properties of diatom nanostructured biosilica in arachnoidiscus sp: micro-optics from mother nature, PLoS One 9 (2014), e103750, https://doi.org/10.1371/JOURNAL.PONE.0103750.

[14] C.C. Lechner, C.F.W. Becker, Silaffins in silica biomineralization and biomimetic silica precipitation, Mar. Drugs 13 (2015) 5297, https://doi.org/10.3390/MD13085297.

[15] I.E. Pamirsky, K.S. Golokhvast, Silaffins of diatoms: from applied biotechnology to biomedicine, Mar. Drugs 11 (2013) 3155, https://doi.org/10.3390/MD11093155.

[16] I.E. Pamirsky, K.S. Golokhvast, Silaffins of diatoms: from applied biotechnology to biomedicine, Mar. Drugs 11 (2013) 3155, https://doi.org/10.3390/MD11093155.

[17] E. Rathinam, S. Govindarajan, S. Rajasekharan, H. Declercq, D. Elewaut, P. de Coster, L. Martens, L. Leybaert, The calcium dynamics of human dental pulp stem cells stimulated with tricalcium silicate-based cements determine their differentiation and mineralization outcome, Sci. Rep. 11 (2021) 1–11, https://doi.org/10.1038/s41598-020-80096-5, 20211–13.

[18] T. Qu, X. Liu, Nano-structured gelatin/bioactive glass hybrid scaffolds for the enhancement of odontogenic differentiation of human dental pulp stem cells, J. Mater. Chem. B 1 (2013) 4764–4772, https://doi.org/10.1039/C3TB21002B.

[19] R. Jugdaohsingh, Silicon and bone health, J. Nutr. Health Aging 11 (2007) 99. /pmc/articles/PMC2658806/ (accessed July 4, 2022).

[20] A.J. Mieszawska, L.D. Nadkarni, C.C. Perry, D.L. Kaplan, Nanoscale control of silica particle formation via silk-silica fusion proteins for bone regeneration, Chem. Mater. 22 (2010) 5780, https://doi.org/10.1021/CM101940U.

[21] D.H. Nam, K. Won, Y.H. Kim, B.I. Sang, A novel route for immobilization of proteins to silica particles incorporating silaffin domains, Biotechnol. Prog. 25 (2009) 1643–1649, https://doi.org/10.1002/BTPR.261.

[22] O. Choi, B.C. Kim, J.H. An, K. Min, Y.H. Kim, Y. Um, M.K. Oh, B.I. Sang, A biosensor based on the self-entrapment of glucose oxidase within biomimetic silica nanoparticles induced by a fusion enzyme, Enzym. Microb. Technol. 49 (2011) 441–445, https://doi.org/10.1016/J.ENZMICTEC.2011.07.005.

[23] T.T. Olmez, E. Yuca, E. Eyupoglu, H.B. Catalak, O. Sahin, U.O.S. Seker, Autonomous synthesis of fluorescent silica biodots using engineered fusion proteins, ACS Omega 3 (2018) 585–594, https://doi.org/10.1021/ACSOMEGA.7B01769/ASSET/IMAGES/LARGE/AO-2017-017695_0004. JPEG.

[24] J.C. Park, D.H. Kim, C.S. Kim, J.H. Seo, R5 peptide-based biosilicification using methyltrimethoxysilane, Biotechnol. Bioproc. Eng. 23 (2018) 11–15, https://doi.org/10.1007/S12257-017-0451-2, 1. 23 (2018.

[25] I.W. Song, H. Park, J.H. Park, H. Kim, S.H. Kim, S. Yi, J. Jaworski, B.I. Sang, Silica formation with nanofiber morphology via helical display of the silaffin R5 peptide on a filamentous bacteriophage, Sci. Rep. 7 (2017) 1, https://doi.org/10.1038/s41598-017-16278-5, 2017.

[26] K. Kjærgaard, H. Hasman, M.A. Schembri, P. Klemm, Antigen 43-mediated autotransporter display, a versatile bacterial cell surface presentation system, J. Bacteriol. 184 (2002) 4197, https://doi.org/10.1128/JB.184.15.4197-4204.2002.

[27] M.W. van der Woude, I.R. Henderson, Regulation and Function of Ag43 (Flu), vol. 62, 2008, pp. 153–169, https://doi.org/10.1146/Annurev.Micro.62.081307.162938, 10.1146/ANNUREV.MICRO.62.081307.162938.

[28] I.R. Henderson, F. Navarro-Garcia, M. Desvaux, R.C. Fernandez, D. Ala'Aldeen, Type V protein secretion pathway: the autotransporter story, Microbiol. Mol. Biol. Rev. 68 (2004) 692–744, https://doi.org/10.1128/MMBR.68.4.692-744.2004/ASSET/783F885B-7D53-4E6D-8C6C-9F9435254D16/ASSETS/GRAPHIC/ZMR0040420690011.JPEG.

[29] M.W. van der Woude, I.R. Henderson, Regulation and function of Ag43 (flu), Annu. Rev. Microbiol. 62 (2008) 153–169, https://doi.org/10.1146/ANNUREV.MICRO.62.081307.162938.

[30] R.E. Ahan, B.M. Klrpat, B. Saltepe, U.Ö.Ş. Şeker, A self-actuated cellular protein delivery machine, ACS Synth. Biol. 8 (2019) 686–696, https://doi.org/10.1021/ACSSYNBIO.9B00062/ASSET/IMAGES/LARGE/SB-2019-000623_0005.JPEG.

[31] K. Kjærgaard, H. Hasman, M.A. Schembri, P. Klemm, Antigen 43-mediated autotransporter display, a versatile bacterial cell surface presentation system, J. Bacteriol. 184 (2002) 4197, https://doi.org/10.1128/JB.184.15.4197-4204.2002.

[32] N. Kröger, R. Deutzmann, M. Sumper, Polycationic peptides from diatom biosilica that direct silica nanosphere formation, Science 286 (1999) 1129–1132, https://doi.org/10.1126/SCIENCE.286.5442.1129/ASSET/0A9BFDC9-BE87-4579-8F6F-3837DE2DF9D3/ASSETS/GRAPHIC/SE4397972005.JPEG, 1979.

[33] R.R. Naik, P.W. Whitlock, F. Rodriguez, L.L. Brott, D.D. Glawe, S.J. Clarson, M.O. Stone, Controlled formation of biosilica structures in vitro, Chem. Commun. (2003) 238–239, https://doi.org/10.1039/B210635C.

[34] E. Jackson, M. Ferrari, C. Cuestas-Ayllon, R. Fernández-Pacheco, J. Perez-Carvajal, J.M. de La Fuente, V. Grazú, L. Betancor, Protein-templated biomimetic silica nanoparticles, Langmuir 31 (2015) 3687–3695, https://doi.org/10.1021/LA504978R/SUPPL_FILE/LA504978R_SI_002.PDF.

[35] L. Senior, M.P. Crump, C. Williams, P.J. Booth, S. Mann, A.W. Perriman, P. Curnow, Structure and function of the silicifying peptide R5, J. Mater. Chem. B 3 (2015) 2607–2614, https://doi.org/10.1039/C4TB01679C.

[36] E.L. Buckle, J. Sampath, N. Michael, S.D. Whedon, C.J.A. Leonen, J. Pfaendtner, G.P. Drobny, C. Chatterjee, Trimethylation of the R5 silica-precipitating peptide increases silica particle size by redirecting orthosilicate binding, Chembiochem 21 (2020) 3208–3211, https://doi.org/10.1002/CBIC.202000264.

[37] O. Choi, B.C. Kim, J.H. An, K. Min, Y.H. Kim, Y. Um, M.K. Oh, B.I. Sang, A biosensor based on the self-entrapment of glucose oxidase within biomimetic silica nanoparticles induced by a fusion enzyme, Enzym. Microb. Technol. 49 (2011) 441–445, https://doi.org/10.1016/J.ENZMICTEC.2011.07.005.

[38] D.H. Nam, K. Won, Y.H. Kim, B.I. Sang, A novel route for immobilization of proteins to silica particles incorporating silaffin domains, Biotechnol. Prog. 25 (2009) 1643–1649, https://doi.org/10.1002/BTPR.261.

[39] R. Mészáros, I. Varga, T. Gilányi, Adsorption of poly(ethyleneimine) on silica surfaces: effect of pH on the reversibility of adsorption, Langmuir 20 (2004) 5026–5029, https://doi.org/10.1021/LA049611L/ASSET/IMAGES/LARGE/LA049611LF00005.JPEG.

[40] G. Mori, G. Brunetti, A. Oranger, C. Carbone, A. Ballini, L. lo Muzio, S. Colucci, C. Mori, F.R. Grassi, M. Grano, Dental pulp stem cells: osteogenic differentiation and gene expression, Ann. N. Y. Acad. Sci. 1237 (2011) 47–52, https://doi.org/10.1111/J.1749-6632.2011.06234.X.

[41] R. Monterubbianesi, M. Bencun, P. Pagella, A. Woloszyk, G. Orsini, T.A. Mitsiadis, A comparative in vitro study of the osteogenic and adipogenic potential of human dental pulp stem cells, gingival fibroblasts and foreskin fibroblasts, Sci. Rep. 9 (1) (2019) 1–13, https://doi.org/10.1038/s41598-018-37981-x, 9 (2019.